

Quasi-Dense Similarity Learning for Multiple Object Tracking

Jiangmiao Pang¹ Linlu Qiu² Xia Li³ Haofeng Chen⁴ Qi Li¹ Trevor Darrell⁵ Fisher Yu³

¹Zhejiang University ²Georgia Institute of Technology ³ETH Zürich
⁴Stanford University ⁵UC Berkeley

Abstract

Similarity learning has been recognized as a crucial step for object tracking. However, existing multiple object tracking methods only use sparse ground truth matching as the training objective, while ignoring the majority of the informative regions on the images. In this paper, we present *Quasi-Dense Similarity Learning*, which densely samples hundreds of region proposals on a pair of images for contrastive learning. We can directly combine this similarity learning with existing detection methods to build *Quasi-Dense Tracking (QDTrack)* without turning to displacement regression or motion priors. We also find that the resulting distinctive feature space admits a simple nearest neighbor search at the inference time. Despite its simplicity, *QDTrack* outperforms all existing methods on MOT, BDD100K, Waymo, and TAO tracking benchmarks. It achieves 68.7 MOTA at 20.3 FPS on MOT17 without using external training data. Compared to methods with similar detectors, it boosts almost 10 points of MOTA and significantly decreases the number of ID switches on BDD100K and Waymo datasets.¹

1. Introduction

Multiple Object Tracking (MOT) is a fundamental and challenging problem in computer vision, widely used in safety monitoring, autonomous driving, video analytics, and other applications. Contemporary MOT methods [3, 5, 47, 56, 46] mainly follow the tracking-by-detection paradigm [38]. That is, they detect objects on each frame and then associate them according to the estimated instance similarity. Recent works [3, 5, 6, 56] show that if the detected objects are accurate, the spatial proximity between objects in consecutive frames, measured by Interaction of Unions (IoUs) or center distances, is a strong prior to associate the objects. However, this location heuristic only works well in simple scenarios. If the objects are occluded or the scenes are

¹The code is available at <https://github.com/SysCV/qdtrack>

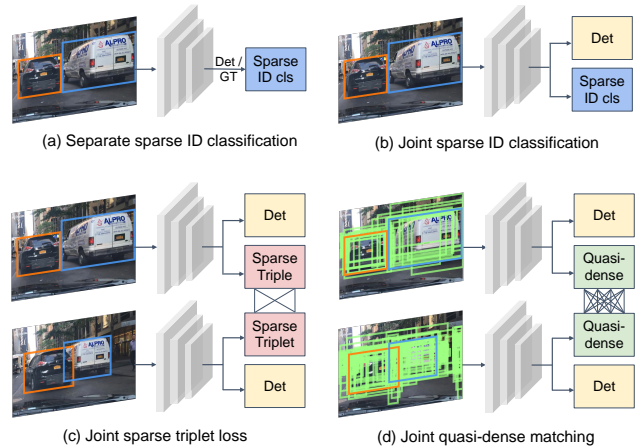


Figure 1: (a) Traditional ReID model that decouples with detector and learns with sparse ID loss; (b) joint learning ReID model with sparse ID loss; (c) joint learning ReID model with sparse triplet loss; (d) our quasi-dense similarity learning.

crowded, this location heuristic can easily lead to mistakes. To remedy this problem, some methods introduce motion estimation [1, 9] or displacement regression [12, 56, 37] to ensure accurate distance estimation.

However, object appearance similarity usually takes a secondary role [29, 47] to strengthen object association or re-identify vanished objects. The search region is constrained to be local neighborhoods to avoid distractions because the appearance features can not effectively distinguish different objects. On the contrary, humans can easily associate the identical objects only through appearance. We conjecture this is because the image and object information is not fully utilized for learning object similarity. As shown in Figure 1, previous methods regard instance similarity learning as a post hoc stage after object detection or only use sparse ground truth bounding boxes as training samples [47]. These processes ignore the majority of the regions proposed on the images. Because objects in an image are rarely iden-

tical to each other, if the object representation is properly learned, a nearest neighbor search in the embedding space should associate and distinguish instances without bells and whistles.

We observe that besides the ground truths and detected bounding boxes, which sparsely distribute on the images, many possible object regions can provide valuable training supervision. They are either close to the ground truth bounding boxes to provide more positive training examples or in the background as negative examples. In this paper, we propose quasi-dense contrastive learning, which densely matches hundreds of regions of interest on a pair of images and learns the metric with contrastive loss. The quasi-dense samples can cover most of the informative regions on the images, providing both more box examples and hard negatives.

Because one sample has more than one positive samples on the reference image, we extend the contrastive learning [14, 41, 49] to multiple positive forms that makes the quasi-dense learning feasible. Each sample is thus trained to distinguish all proposals on the other image simultaneously. This contrast provides stronger supervision than using only the handful ground truth labels and enhances the instance similarity learning.

The inference process, which maintains the matching candidates and measures the instance similarity, also plays an important role in the tracking performance. Besides similarity, MOT also needs to consider false positives, id switches, new appeared objects, and terminated tracks. To tackle the missing targets with our similarity metric, we include backdrops, the unmatched objects in the last frame, for matching and use *bi-directional softmax* to enforce the bi-directional consistency. The no target objects lack the consistency thus has low similarity scores to any objects. To track the multiple targets, we also conduct duplicate removal to filter the matching candidates.

Quasi-dense contrastive learning can be easily used with most existing detectors since generating region of interests is widely used in object detection algorithms. In this paper, we apply our method to Faster R-CNN [39] along with a lightweight embedding extractor and residual networks [17] and build *Quasi-Dense Tracking* (QDTrack) models. We conduct extensive experiments on MOT [31], BDD100K [53], Waymo [43], and TAO [10] tracking benchmarks. Despite its simplicity, QDTrack outperforms all existing methods without bells and whistles. It achieves 68.7 MOTA on MOT17 at 20.3 FPS without using external training data. Moreover, it boosts almost 10 points of MOTA and significantly decreases the number of ID switches on BDD100K and Waymo datasets, establishing solid records on these brand-new large-scale benchmarks. QDTrack allows end-to-end training, thereby simplifying the training and testing procedures of multi-object tracking frameworks. The simplicity and effectiveness shall benefit further research.

2. Related work

Recent developments in multiple object tracking [25] follow the tracking-by-detection paradigm [38]. These approaches present different methods to estimate the instance similarity between detected objects and previous tracks, then associate objects as a bipartite matching problem [33].

Location and motion in MOT The spatial proximity has been proven effective to associate objects in consecutive frames [5, 6]. However, they cannot do well in complicated scenarios such as crowd scenes. Some methods use motion priors, such as Kalman Filter [5, 54], optical flow [50], and displacement regression [18, 12], to ensure accurate distance estimations. In contrast to the old paradigm that detects objects and predicts displacements separately, Detect & Track [12] is the first work that jointly optimizes object detection and tracking modules. It predicts the displacements of the objects in consecutive frames and associates the objects with the Viterbi algorithm. Tracktor [3] directly adopts a detector as a tracker. CenterTrack [56] and Chained-Tracker [37] predict the object displacements with pair-wise inputs to associate the objects. Although these methods show promising results, they [47, 3] still need an extra re-identification model as complementary to re-identify vanished objects, making the entire framework complicated.

Appearance similarity in MOT To exploit instance appearance similarity to strengthen tracking and re-identify vanished objects, some methods directly use an independent model [22, 24, 51, 42, 40, 32, 47, 3] or add an extra embedding head to the detector for end-to-end training [52, 29, 46, 55]. However, they still learn the appearance similarity following the practice in image similarity learning, then measure the instance similarity by cosine distance. That is, they train the model either as a n -classes classification problem [47] where n equals to the number of identities in the whole training set or using triplet loss [20]. The classification problem is hard to extend to large-scale datasets, while the triplet loss only compares each training sample with two other identities. These rudimentary training samples and objectives leave instance similarity learning not fully explored in MOT. Meanwhile, they still heavily rely on motion models and displacement predictions to track objects, and the appearance similarity only takes the secondary role.

In contrast to these methods, QDTrack learns the instance similarity from dense-connected contrastive pairs and associates objects from the feature space with a simple nearest neighbor search. QDTrack has higher performance but with a simpler framework. The promising results prove the power of quasi-dense similarity learning in multiple object tracking.

Contrastive learning Contrastive learning and its variants [2, 19, 34, 45, 49, 15, 8, 44] have shown promising performance in self-supervised representation learning. However, it does not draw much attention when learning the instance similarity in multiple object tracking. In this pa-

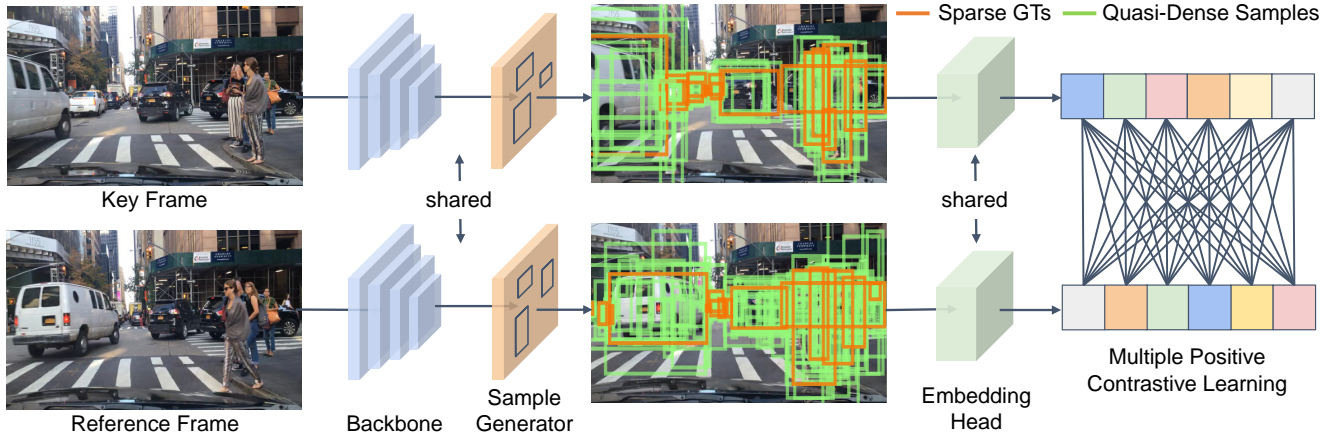


Figure 2: The training pipeline of our method. We apply dense matching between quasi-dense samples on the pair of images and optimize the network with multiple positive contrastive learning.

per, we supervise dense matched quasi-dense samples with multiple positive contrastive learning by the inspiration of [44]. In contrast to these image-level contrastive methods, our method allows multiple positive training, while these methods can only handle the case when there is only one positive target. The promising results of our method shall draw the attention to contrastive learning in the multiple object tracking community.

3. Methodology

We propose *quasi-dense matching* to learn the feature embedding space that can associate identical objects and distinguish different objects for online multiple object tracking. We define *dense matching* to be matching between box candidates at all pixels, and *quasi-dense* means only considering the potential object candidates at informative regions. Accordingly, *sparse matching* means the method only considers ground truth labels as matching candidates when learning object association. The main ingredients of using quasi-dense matching for multiple object tracking are object detection, instance similarity learning, and object association.

3.1. Object detection

Our method can be easily coupled with most existing detectors and admit end-to-end training. In this paper, we take Faster R-CNN [39] with Feature Pyramid Network (FPN) [26] as an example, while we can also apply other detectors with minor modifications. Faster R-CNN is a two-stage detector that uses Region Proposal Network (RPN) to generate Region of Interests (RoIs). It then localizes and classifies the regions to obtain semantic labels and locations. Based on Faster R-CNN, FPN exploits lateral connections to build the top-down feature pyramid and tackles the scale-variance problem. The entire network is optimized with a

multi-task loss function

$$\mathcal{L}_{\text{det}} = \mathcal{L}_{\text{rpn}} + \lambda_1 \mathcal{L}_{\text{cls}} + \lambda_2 \mathcal{L}_{\text{reg}}, \quad (1)$$

where the RPN loss \mathcal{L}_{rpn} , classification loss \mathcal{L}_{cls} , regression loss \mathcal{L}_{reg} remain the same as the original paper [39]. The loss weights λ_1 and λ_2 are set to 1.0 by default.

3.2. Quasi-dense similarity learning

We use the region proposals generated by RPN to learn the instance similarity with quasi-dense matching. As shown in Figure 2, given a key image I_1 for training, we randomly select a reference image I_2 from its temporal neighborhood. The neighbor distance is constrained by an interval k , where $k \in [-3, 3]$ in our experiments. We use RPN to generate RoIs from the two images and RoI Align [16] to obtain their feature maps from different levels in FPN according to their scales [26]. We add an extra lightweight embedding head, in parallel with the original bounding box head, to extract features for each RoI. An RoI is defined as positive to an object if they have an IoU higher than α_1 , or negative if they have an IoU lower than α_2 . α_1 and α_2 are 0.7 and 0.3 in our experiments. The matching of RoIs on two frames is positive if the two regions are associated with the same object and negative otherwise.

Assume there are V samples on the key frame as training samples and K samples on the reference frame as contrastive targets. For each training sample, we can use the non-parametric softmax [49, 34] with cross-entropy to optimize the feature embeddings

$$\mathcal{L}_{\text{embed}} = -\log \frac{\exp(\mathbf{v} \cdot \mathbf{k}^+)}{\exp(\mathbf{v} \cdot \mathbf{k}^+) + \sum_{\mathbf{k}^-} \exp(\mathbf{v} \cdot \mathbf{k}^-)}, \quad (2)$$

where \mathbf{v} , \mathbf{k}^+ , \mathbf{k}^- are feature embeddings of the training sample, its positive target, and negative targets in K . The overall

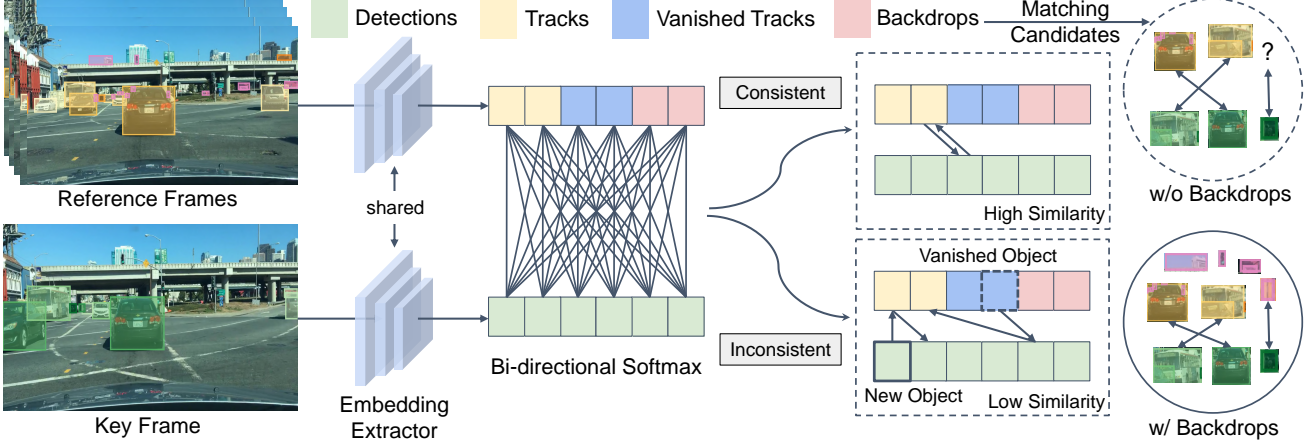


Figure 3: The testing pipeline of our method. We maintain the matching candidates and use bi-softmax to measure the instance similarity so that we can associate objects with a simple nearest neighbour search in the feature space.

embedding loss is averaged across all training samples, but we only illustrate one training sample for simplicity.

We apply dense matching between RoIs on the pairs of images, namely, each sample on I_1 is matched to all samples on I_2 , in contrast to only using sparse sample crops, mostly ground truth boxes, to learn instance similarity in previous works [4, 20]. Each training sample on the key frame has more than one positive targets on the reference frame, so Eq. 2 can be extended as

$$\mathcal{L}_{\text{embed}} = - \sum_{\mathbf{k}^+} \log \frac{\exp(\mathbf{v} \cdot \mathbf{k}^+)}{\exp(\mathbf{v} \cdot \mathbf{k}^+) + \sum_{\mathbf{k}^-} \exp(\mathbf{v} \cdot \mathbf{k}^-)}. \quad (3)$$

However, this equation does not treat positive and negative targets fairly. Namely, each negative one is considered multiple times while only once for positive counterparts. Alternatively, we can first reformulate Eq. 2 as

$$\mathcal{L}_{\text{embed}} = \log[1 + \sum_{\mathbf{k}^-} \exp(\mathbf{v} \cdot \mathbf{k}^- - \mathbf{v} \cdot \mathbf{k}^+)]. \quad (4)$$

Then in the multi-positive scenario, it can be extended by accumulating the positive term as

$$\mathcal{L}_{\text{embed}} = \log[1 + \sum_{\mathbf{k}^+} \sum_{\mathbf{k}^-} \exp(\mathbf{v} \cdot \mathbf{k}^- - \mathbf{v} \cdot \mathbf{k}^+)]. \quad (5)$$

We further adopt L2 loss as an auxiliary loss

$$\mathcal{L}_{\text{aux}} = \left(\frac{\mathbf{v} \cdot \mathbf{k}}{\|\mathbf{v}\| \cdot \|\mathbf{k}\|} - c \right)^2, \quad (6)$$

where c is 1 if the match of two samples is positive and 0 otherwise. Note the auxiliary loss aims to constrain the logit magnitude and cosine similarity instead of improving the performance.

The entire network is joint optimized under

$$\mathcal{L} = \mathcal{L}_{\text{det}} + \gamma_1 \mathcal{L}_{\text{embed}} + \gamma_2 \mathcal{L}_{\text{aux}}, \quad (7)$$

where γ_1 and γ_2 are set to 0.25 and 1.0 by default in this paper. We sample all positive pairs and three times more negative pairs to calculate the auxiliary loss.

3.3. Object association

Tracking objects across frames purely based on object feature embeddings is not trivial. For example, if an object has no target or more than one target during matching, the nearest search will be ambiguous. In other words, an object should have only one target in the matching candidates. However, the actual tracking process is complex. The false positives, id switches, newly appeared objects, and terminated tracks all increase the matching uncertainty. We observe that our inference strategy, including ways of maintaining the matching candidates and measuring the instance similarity, can mitigate these problems.

Bi-directional softmax Our main inference strategy is bi-directional matching in the embedding space. Figure 3 shows our testing pipeline. Assume there are N detected objects in frame t with feature embeddings \mathbf{n} , and M matching candidates with feature embeddings \mathbf{m} from the past x frames, the similarity \mathbf{f} between the objects and matching candidates is obtained by bi-directional softmax (bi-softmax):

$$\mathbf{f}(i, j) = \left[\frac{\exp(\mathbf{n}_i \cdot \mathbf{m}_j)}{\sum_{k=0}^{M-1} \exp(\mathbf{n}_i \cdot \mathbf{m}_k)} + \frac{\exp(\mathbf{n}_i \cdot \mathbf{m}_j)}{\sum_{k=0}^{N-1} \exp(\mathbf{n}_k \cdot \mathbf{m}_j)} \right] / 2. \quad (8)$$

The high score under bi-softmax will satisfy a bi-directional consistency. Namely, the two matched objects should be each other's nearest neighbor in the embedding space. The instance similarity \mathbf{f} can directly associate objects with a simple nearest neighbor search.

Table 1: Results on MOT16 and MOT17 object tracking benchmark test set. Note that we do not use extra data for training. \uparrow means higher is better, \downarrow means lower is better. * means external data besides COCO and ImageNet is used.

Dataset	Method	MOTA \uparrow	IDF1 \uparrow	MOTP \uparrow	MT \uparrow	ML \downarrow	FP \downarrow	FN \downarrow	IDs \downarrow
MOT16	TAP [57]	64.8	73.5	78.7	292	164	12980	50635	571
	CNNMTT [30]	65.2	62.2	78.4	246	162	6578	55896	946
	POI* [54]	66.1	65.1	79.5	258	158	5061	55914	3093
	TubeTK_POI* [35]	66.9	62.2	78.5	296	122	11544	47502	1236
	CTrackerV1 [37]	67.6	57.2	78.4	250	175	8934	48305	1897
	Ours	69.8	67.1	79.0	316	150	9861	44050	1097
MOT17	Tracktor++v2 [3]	56.3	55.1	78.8	498	831	8866	235449	1987
	Lif_T* [21]	60.5	65.6	78.3	637	791	14966	206619	1189
	TubeTK* [35]	63.0	58.6	78.3	735	468	27060	177483	4137
	CTrackerV1 [37]	66.6	57.4	78.2	759	570	22284	160491	5529
	CenterTrack* [56]	67.8	64.7	78.4	816	579	18498	160332	3039
	Ours	68.7	66.3	79.0	957	516	26589	146643	3378

No target cases Objects without a target in the feature space should not be matched to any candidates. Newly appeared objects, vanished tracks, and some false positives fall into this category. The bi-softmax can tackle this problem directly, as it is hard for these objects to obtain bi-directional consistency, leading to low matching scores. If a newly detected object has high detection confidence, it can start a new track. However, previous methods often directly drop the objects that do not match any tracks. We argue that despite most of them are false positives, they are still useful regions that the following objects are likely to match. We name these unmatched objects *backdrops* and keep them during matching. Experiments show that backdrops can reduce the number of false positives.

Multi-targets cases Most states of the art detectors only do intra-class duplicate removal by None Maximum Suppression (NMS). Consequently, some objects may have different categories but the same locations. In most cases, only one of these objects is true positive while the others not. This process can boost the object recall and contribute to a high mean Average Precision (mAP) [11, 27]. However, it will create duplicate feature embeddings. To handle this issue, we do inter-class duplicate removal by NMS. The IoU threshold for NMS is 0.7 for objects with high detection confidence (larger than 0.5) and 0.3 for objects with low detection confidence (lower than 0.5).

4. Experiments

We first conduct experiments on MOT [31], the most popular benchmark in multiple object tracking to compare with recent tracking works. We also like to test on larger scale and more diverse datasets to study the efficacy of quasi-dense similarity learning. Therefore, we conduct experiments on the brand-new large-scale BDD100K, Waymo, and TAO

tracking benchmarks, and establish competitive records. We hope our efforts can facilitate further research in multiple object tracking. We also show the generalization ability of our method on the BDD100K segmentation tracking benchmark.

4.1. Datasets

MOT We perform experiments on two MOT benchmarks: MOT17 and MOT16 [31]. The dataset contains 7 videos (5,316 images) for training and 7 videos (5,919 images) for testing. Only pedestrians are evaluated in this benchmark. The video frame rate is 14 - 30 FPS.

BDD100K We use BDD100K [53] detection training set and tracking training set for training, and tracking validation/testing set for testing. It annotates 8 categories for evaluation. The detection set has 70,000 images. The tracking set has 1,400 videos (278k images) for training, 200 videos (40k images) for validation, and 400 videos (80k images) for testing. The images in the tracking set are annotated per 5 FPS with a 30 FPS video frame rate.

Waymo Waymo open dataset [43] contains images from 5 cameras associated with 5 different directions: front, front left, front right, side left, and side right. There are 3,990 videos (790k images) for training, 1,010 videos (200k images) for validation, and 750 videos (148k images) for testing. It annotates 3 classes for evaluation. The videos are annotated in 10 FPS.

TAO TAO dataset [10] annotates 482 classes in total, which are the subset of LVIS dataset [13]. It has 400 videos, 216 classes in the training set, 988 videos, 302 classes in the validation set, and 1419 videos, 369 classes in the test set. The classes in train, validation, and test sets may not overlap. The videos are annotated in 1 FPS. The objects in TAO are in a long-tailed distribution that half of the objects are person and 1 / 6 of the objects are car.

Table 2: Results on BDD100K tracking validation and test set. mMOTA and mIDF1 are averages over 8 categories while MOTA and IDF1 indicates the overall performance without considering categories. Our method outperforms the champion of BDD100K 2020 Tracking Challenge (madamada) only with a simple single model.

Method	Split	mMOTA \uparrow	mIDF1 \uparrow	MOTA \uparrow	IDF1 \uparrow	FN \downarrow	FP \downarrow	ID Sw. \downarrow	MT \uparrow	ML \downarrow	mAP \uparrow
Yu <i>et al.</i> [53]	val	25.9	44.5	56.9	66.8	122406	52372	8315	8396	3795	28.1
Ours	val	36.6	50.8	63.5	71.5	108614	46621	6262	9481	3034	32.6
Yu <i>et al.</i> [53]	test	26.3	44.7	58.3	68.2	213220	100230	14674	16299	6017	27.9
DeepBlueAI	test	31.6	38.7	56.9	56.0	292063	35401	25186	10296	12266	-
madamada	test	33.6	43.0	59.8	55.7	209339	76612	42901	16774	5004	-
Ours	test	35.5	52.3	64.3	72.3	201041	80054	10790	17353	5167	31.8

Table 3: Results on Waymo tracking validation set using py-motmetrics library (top)² and test set using official evaluation. * indicates methods using undisclosed detectors.

Method	Split	Category	MOTA \uparrow	IDF1 \uparrow	FN \downarrow	FP \downarrow	ID Sw. \downarrow	MT \uparrow	ML \downarrow	mAP \uparrow
IoU baseline [29]	val	Vehicle	38.25	-	-	-	-	-	-	45.78
Tracktor++ [3, 29]	val	Vehicle	42.62	-	-	-	-	-	-	42.41
RetinaTrack [29]	val	Vehicle	44.92	-	-	-	-	-	-	45.70
Ours	val	Vehicle	55.6	66.2	514548	214998	24309	17595	5559	49.5
Ours	val	All	44.0	56.8	674064	264886	30712	21410	7510	40.1

Method	Split	Category	MOTA/L1 \uparrow	FP/L1 \downarrow	MisM/L1 \downarrow	Miss/L1 \downarrow	MOTA/L2 \uparrow	FP/L2 \downarrow	MisM/L2 \downarrow	Miss/L2 \downarrow
Tracktor [23, 43]	test	Vehicle	34.80	10.61	14.88	39.71	28.29	8.63	12.10	50.98
CascadeRCNN-SORTv2*	test	All	50.22	7.79	2.71	39.28	44.15	6.94	2.44	46.46
HorizonMOT*	test	All	51.01	7.52	2.44	39.03	45.13	7.13	2.25	45.49
Ours (ResNet-50)	test	All	49.40	7.41	1.46	41.74	43.88	7.10	1.31	48.21
Ours (ResNet-101 + DCN)	test	All	51.18	7.64	1.45	39.73	45.09	7.20	1.31	46.41

4.2. Implementation details

We use ResNet-50 [17] as backbone. We select 128 RoIs from the key frame as training samples, and 256 RoIs from the reference frame with a positive-negative ratio of 1.0 as contrastive targets. We use IoU-balanced sampling [36] to sample RoIs. We use *4conv-1fc* head with group normalization [48] to extract feature embeddings. The channel number of embedding features is set to 256 by default. We train our models with a total batch size of 16 and an initial learning rate of 0.02 for 12 epochs. We decrease the learning rate by 0.1 after 8 and 11 epochs.

Here, we first talk about the other common practice of our method if not specified mentioned below. We use the original scale of the images for training and inference. We do not use any other data augmentation methods except random horizontal flipping. We use a model pre-trained on ImageNet for training. When conducting online joint object detection and tracking, we initialize a new track if its detection confidence is higher than 0.8. Other confidence thresholds are all set as 0.5 in this paper if not mentioned. The objects can be associated only when they are classified as the same category. The feature embeddings of each identity

are updated online with a momentum of 0.8.

For fair comparison with recent works, we follow the practice [46] on MOT17 that randomly resizes and crops the longer side of the images to 1088 and does not change the aspect ratio at the training and inference time. Other data augmentation includes random horizontal flipping and color jittering, which is the common practice in [46, 56, 37]. We do not use extra data for training except a pre-trained model from COCO. Note that COCO is not considered as additional training data by the official rules and widely used in most methods.

On TAO, we randomly select a scale between 640 to 800 to resize the shorter side of images during training. At inference time, the shorter side of the images are resized to 800. We use a LVIS [13] pre-trained model, consistent with the implementation of [10]. However, we observe severe over-fitting problem when training on the training videos of TAO, which hurts the detection performance. So we freeze the detection model and only fine-tune the embedding head to extract instance representations.

4.3. Main results

Our method outperforms all existing methods on aforementioned benchmarks without bells and whistles. The per-

²<https://github.com/cheind/py-motmetrics>

Table 4: Ablation studies on quasi-dense matching and the inference strategy. All models are comparable on detection performance. D. R. means duplicate removal. (P) means results of the class “pedestrian”.

Quasi-Dense		Metric	Matching candidates		MOTA ↑	IDF1 ↑	mMOTA ↑	mIDF1 ↑	MOTA(P) ↑	IDF1(P) ↑
one-positive	multi-positive		D. R.	Backdrops						
-	-	<i>cosine</i>	-	-	60.4	63.0	34.0	47.9	37.6	49.7
✓	-	<i>cosine</i>	-	-	61.5	66.8	35.5	50.0	40.5	52.7
-	✓	<i>cosine</i>	-	-	62.5	67.8	36.2	50.0	44.0	54.3
-	✓	<i>bi-softmax</i>	-	-	62.9	70.0	35.4	48.5	45.5	58.8
-	✓	<i>bi-softmax</i>	✓	-	63.2	70.1	36.4	50.4	45.5	58.3
-	✓	<i>bi-softmax</i>	✓	✓	63.5	71.5	36.6	50.8	46.7	60.2
					+3.1	+8.5	+2.6	+2.9	+9.1	10.5

Table 5: Ablations studies on location and motion cues on the BDD100K tracking validation set. All experiments use the same detector for fair comparisons.

Appearance	IoU	Motion	Regression	mMOTA ↑	mIDF1 ↑
-	✓	-	-	26.3	36.0
-	✓	✓	-	27.7	38.5
-	✓	-	✓	28.6	39.3
✓	-	-	-	36.6	50.8
✓	✓	-	-	36.3	49.8
✓	✓	✓	-	36.4	49.9
✓	✓	-	✓	36.4	50.1

formance are evaluated according to the official metrics of each benchmark.

MOT The results on MOT17 and MOT16 benchmark are shown in Table 1. Our model achieves the best MOTA of 68.7% and IDF1 of 66.3% on the MOT17 and best MOTA of 69.8% on MOT16 without using external training data. We outperform the recent state of the art tracker CenterTrack [56] by 0.9 points on MOTA and 1.6 points on IDF1 on MOT17 benchmark, showing the effectiveness of our method.

BDD100K The main results on BDD100K tracking validation and testing sets are in Table 2. The mMOTA and mIDF1, which represent object coverage and identity consistency respectively, are 36.6% and 50.8% on the validation set, and 35.5% and 52.3% on the testing set. On the two sets, our method outperforms the baseline benchmark method by 10.7 points and 9.2 points in terms of mMOTA, and 6.3 points and 7.6 points in terms of mIDF1 respectively. We also outperform the champion of BDD100K 2020 MOT Challenge (madamada) by a large margin but with a simpler detector. The significant advancements demonstrate that our method enables more stable object tracking.

Waymo Table 3 shows our main results on Waymo open dataset. We report the results on the validation set following the setup of RetinaTrack [29], which only conduct experiments on the vehicle class. We also report the overall performance for future comparison. We report the results

on the test set via official rules. Our method outperforms all baselines on both validation set and test set. We obtain a MOTA of 44.0% and a IDF1 of 56.8% on the validation set. We also obtain a MOTA/L1 of 49.40% and a MOTA/L2 of 43.88% on the test set. The performance of vehicle on the validation set is 10.7, 13.0, and 17.4 points higher than RetinaTrack [29], Tractor++ [3, 29], and IoU baseline [29], respectively. Our model with ResNet-101 and deformable convolution (DCN) has the state-of-the-art performance on the test benchmark which is on par with the champion of Waymo 2020 2D Tracking Challenge (HorizonMOT) but only with a simple single model.

TAO We obtain 16.1 points and 12.4 points of AP50 on the validation and test set, respectively. The results are 2.9 points and 2.2 points higher than TAO’s solid baseline, which are 13.2 points and 10.2 points respectively. Although we only boost the overall performance by 2 - 3 points, we observe that we outperform the baseline by a large margin on frequent classes, that is, 38.6 points vs. 18.5 points on person. This improvement is buried by the average across the entire hundreds of classes. It shows that the crucial part on TAO is still how to improve the tracking on tail classes, which should be a meaningful direction for further research.

4.4. Ablation studies

We conduct ablation studies on BDD100K validation set, where we investigate the importance of the major model components for training and testing procedures.

Importance of quasi-dense matching The results are presented in the top sub-table of Table 4. MOTA and IDF1 are calculated over all instances without considering categories as overall evaluations. We use cosine distance to calculate the similarity scores during the inference procedure. Compared to learning with sparse ground truths, quasi-dense tracking improves the overall IDF1 by 4.8 points (63.0% to 67.8%). The significant improvement on IDF1 indicates quasi-dense tracking greatly improves the feature embeddings and enables more accurate associations.

We then analyze the improvements in detail. In the table, we can observe that when we match each training sample

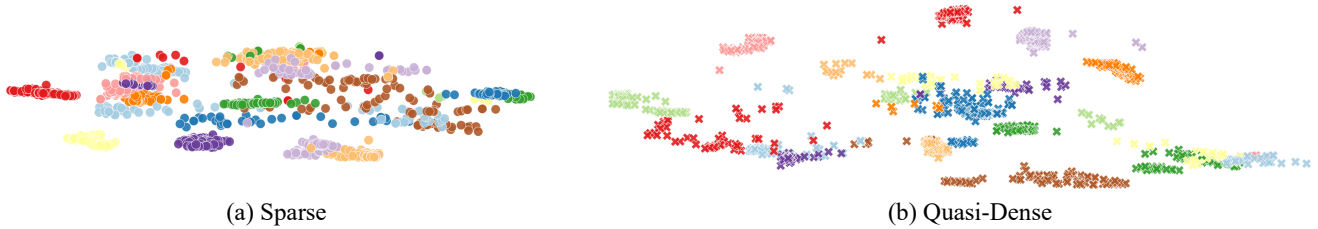


Figure 4: Visualizations of instance embeddings with (a) sparse matching and (b) quasi-dense matching using t-SNE.

to more negative samples and train the feature space with Equation 2, the IDF1 is significantly improved by 3.4 points. This improvement contributes 70% to the total improved 4.8 points IDF1. This experiment shows that more contrastive targets, even most of them are negative samples, can improve the feature learning process. The multiple-positive contrastive learning following Equation 5 further improves the IDF1 by 1 point (66.8% to 67.8%).

Importance of bi-softmax We investigate how different inference strategies influence the performance. As shown in the bottom part of Table 4, replacing cosine similarity by bi-softmax improves overall IDF1 by 2.2 points and the IDF1 of pedestrian by 4.5 points. This experiment also shows that the one-to-one constraint further strengthens the estimated similarity.

Importance of matching candidates Duplicate removal and backdrops improve IDF1 by 1.5 points. Overall, our training and inference strategies improve the IDF1 by 8.5 points (63.0% to 71.5%). The total number of ID switches is decreased by 30%. Especially, the MOTA and IDF1 of pedestrian are improved by 9.1 points and 10.5 points respectively, which further demonstrate the power of quasi-dense contrastive learning.

Combinations with motion and location Finally, we try to add the location and motion priors to understand whether they are still helpful when we have good feature embeddings for similarity measure. These experiments follow the procedures in Tractor [3] and use the same detector for fair comparisons. As shown in Table 5, without appearance features, the tracking performance is consistently improved with the introduction of additional information. However, these cues barely enhance the performance of our approach. Our method yields the best results when only using appearance embeddings. The results indicate that our instance feature embeddings are sufficient for multiple object tracking with the effective quasi-dense matching, which greatly simplify the testing pipeline.

Inference speed To understand the runtime efficiency, we profile our method on NVIDIA Tesla V100. Because it only adds a lightweight embedding head to Faster R-CNN, our method only bring marginal inference cost overhead. With an input size of 1296×720 and a ResNet-50 backbone on BDD100K, the inference FPS is 16.4. With an input size

Table 6: Results on the BDD100K segmentation tracking val set. I: ImageNet. C: COCO. S: Cityscapes. B: BDD100K.

Method	Pretrained	mAP \uparrow	mMOTSA \uparrow	mMOTSP \uparrow	mIDF1 \uparrow	ID sw. \downarrow
SortIoU	I, C, S	22.2	10.3	59.9	21.8	15951
Yang et al. [52]	I, C, S	22.0	12.3	59.9	26.2	9116
Ours	I, C, S	22.4	18.2	59.6	35.1	2305
Ours-fix	I, B	25.5	22.5	65.8	43.9	1591

of 1088×608 and a ResNet-50 backbone on MOT17, the inference FPS is 20.3.

4.5. Embedding visualizations

We visualize the instance embeddings that trained with sparse matching and quasi-dense matching using t-SNE in Figure 4. The same instance is shown with the same color. We observe that it is easier to separate objects in the feature space of quasi-dense matching.

4.6. Segmentation tracking

We show the generalization ability of our method by extending it to instance segmentation tracking. BDD100K provides a subset for the segmentation tracking task. There are 154 videos (30,817 images) in the training set and 32 videos (6,475 images) in the validation set. Table 6 shows the results on BDD100K segmentation tracking task. "-fix" means adopting the pretrained model from the BDD100K tracking set, fixing the existing parts, and only training the added mask head.

5. Conclusion

We present QDTrack, a tracking method based on quasi-dense matching for instance similarity learning. In contrast to previous methods that use sparse ground-truth matching as similarity supervision, we learn instance similarity from hundreds of region proposals on pairs of images, and train the feature embeddings with multiple positive contrastive learning. In the resulting feature space, a simple nearest neighbor search can distinguish instances without bells and whistles. Our method can be easily coupled with most of the existing detectors and trained end-to-end for multiple object tracking and segmentation tracking.

A. Appendix

In this appendix, we present additional experiments, investigate oracle performance, analyze failure cases, and show some patch visualizations.

B. Supplementary experiments

MOT17 with public detectors Following the strategy in Tracktor [3] and CenterTrack [56], we evaluate our method with public detectors on MOT17. That is, a new trajectory is only initialized from a public detection bounding box. As shown in Table 8, our method outperforms existing results by a large margin. Our method outperforms CenterTrack by 3.1 points on MOTA and 5.5 points on IDF1.

TAO Table 7 presents detailed results on the TAO [10] dataset. Although QDTrack does not perform zero-shot and few-shot learning for the long-tail categories, our method is still a stronger baseline method on this dataset and paves the way for future studies.

C. Oracle analysis

We investigate the performances of two types of oracles: detection oracle and tracking oracle on BDD100K tracking validation set. For detection oracle, we directly extract feature embeddings of the ground truth objects in each frame and associate them using our method. For tracking oracle, we use ground truth tracking labels to associate the detected objects.

Detection oracle The results are shown in Table 9. We can observe that all MOTAs are higher than 94%, and some of them are even close to 100%. This is because we use the ground truth boxes directly so that the number of false negatives and false positives are close to 0.

Table 7: Results on TAO challenge benchmark.

Method	Split	AP50	AP75	AP	AP50(S)	AP50(M)	AP50(L)
SORT_TAO [10]	<i>val</i>	13.2	-	-	-	-	-
Ours	<i>val</i>	16.1	5.0	7.0	2.4	4.6	9.6
SORT_TAO [10]	<i>test</i>	10.2	4.4	4.9	7.7	8.2	15.2
Ours	<i>test</i>	12.4	4.5	5.2	3.7	8.3	18.8

Table 8: Results on MOT17 test set with public detector. Note that we do not use extra data for training. \uparrow means higher is better, \downarrow means lower is better. * means external data besides COCO and ImageNet is used.

Dataset	Method	MOTA \uparrow	IDF1 \uparrow	MOTP \uparrow	MT \uparrow	ML \downarrow	FP \downarrow	FN \downarrow	IDs \downarrow
Public MOT17	Tracktor++v2 [3]	56.3	55.1	78.8	498 (21.1)	831 (35.3)	8866	235449	1987 (34.1)
	GSM_Tracktor [28]	56.4	57.8	77.9	523 (22.2)	813 (34.5)	14379	230174	1485 (25.1)
	MPNTrack* [7]	58.8	61.7	78.6	679 (28.8)	788 (33.5)	17413	213594	1185 (19.1)
	Lif_T* [21]	60.5	65.6	78.3	637 (27.0)	791 (33.6)	14966	206619	1189 (18.8)
	CenterTrackPub* [56]	61.5	59.6	78.9	621 (26.4)	752 (31.9)	14076	200672	2583 (40.1)
	Ours	64.6	65.1	79.6	761 (32.3)	666 (28.3)	14103	182998	2652 (39.3)

The metric IDF1 and ID Switches can measure the performance of identity consistency. The average IDF1 over the 8 classes is 88.8%, which is 38 points higher than our result. The gaps on classes “car” and “pedestrian” are only 11.1 points and 19.3 points between oracle results and our results respectively, while gaps on other classes are exceeding 30 points. These results show that if highly accurate detection results are provided, our method can obtain robust feature embeddings and associate objects effectively. However, the huge performance gaps also indicate the demand of promoting detection algorithms in the video domain. We also notice that the total number of ID switches in the oracle experiment is higher than ours. This is due to the high object recalls in the oracle experiments, as more detected instances may introduce more ID switches accordingly.

Tracking oracle The results are shown in Table 10. We can observe that when associating object directly with tracking labels, the mIDF1 is only boosted by 4.3 points. This promising oracle analysis shows the effectiveness of our method and indicates that our method is bounded more by detection performance than tracking performance.

D. Failure case analysis

Our method can distinguish different instances even they are similar in appearance. However, there are still some failure cases. We show them below with figures, in which we use yellow color to represent false negatives, red color to represent false positives, and cyan color to represent ID switches. The float number at the corner of each box indicates the detection score, while the integer indicates the object identity number. We use green dashed box to highlight the objects we want to emphasize.

Object classification Inaccurate classification confidence is the main distraction for the association procedure because false negatives and false positives destroy the one-to-one matching constraint. As shown in Figure 5, the false negatives are mainly small objects or occluded objects under crowd scenes. The false positives are objects that have similar appearances to annotated objects, such as persons in the mirror or advertising board, etc.

Inaccurate object category is a less frequent distraction

Table 9: Detection oracle analysis. The numbers in the round brackets mean the gaps between oracle results and our results.

Category	Set	MOTA \uparrow	IDF1 \uparrow	MOTP \uparrow	FN \downarrow	FP \downarrow	ID Sw. \downarrow	MT \uparrow	ML \downarrow
Pedestrian	val	94.3	79.5 (+19.3)	99.8	1	1	3226	3506	0
Rider	val	95.8	88.5 (+40.4)	99.9	0	0	107	134	0
Car	val	97.7	86.1 (+11.1)	99.9	0	0	7716	13189	0
Bus	val	99.2	93.0 (+31.2)	100.0	0	0	72	196	0
Truck	val	98.8	90.3 (+33.8)	100.0	0	0	340	726	0
Bicycle	val	88.2	79.5 (+31.8)	98.7	8	8	470	243	0
Motorcycle	val	97.0	94.5 (+37.8)	99.8	0	0	27	44	0
Train	val	99.4	98.7 (+98.7)	100.0	0	0	2	6	0
All (average)	val	96.3	88.8 (+38.0)	99.8	9	9	11960	18044	0

Table 10: Tracking oracle analysis. The numbers in the round brackets mean the gaps between oracle results and our results.

Category	Set	MOTA \uparrow	IDF1 \uparrow	MOTP \uparrow	FN \downarrow	FP \downarrow	ID Sw. \downarrow	MT \uparrow	ML \downarrow
Pedestrian	val	54.7	71.2 (+11.0)	77.6	14990	10095	755	1835	367
Rider	val	31.4	52.6 (+4.5)	76.6	1390	242	115	16	56
Car	val	74.3	82.9 (+7.9)	84.1	54585	31014	2309	8759	1141
Bus	val	38.2	65.8 (+4.0)	86.1	3532	2031	57	61	41
Truck	val	37.0	60.9 (+4.4)	84.7	12719	4259	247	149	239
Bicycle	val	30.6	55.6 (+7.9)	75.4	2031	714	125	60	58
Motorcycle	val	14.6	51.7 (-5.0)	76.4	443	292	35	10	18
Train	val	-0.6	0.0 (+0.0)	0.0	308	2	0	0	6
All (average)	val	35.0	55.1 (+4.3)	70.1	89998	48649	3643	10890	1926

caused by classification. The class of the instance may switch between different categories, which mostly belong to the same super-category. Figure 6 shows an example. The category of the highlighted object changes from “rider” to “pedestrian” when the bicycle is occluded. Our method fails in this case because we require the associated objects have the same category.

These failure cases caused by object classification suggest the improvements on video object detection algorithms. We can exploit temporal or tracking information to improve the detectors, thus obtaining better tracking performance.

Object truncation/occlusion Object truncation/occlusion causes inaccurate object localization. As shown in Figure 7, the highlighted objects are truncated by other objects. The detector detects two objects. One of them is a false positive box that only covers a part of the object. The other one is a box with a lower detection score but covers the entire object. This case may influence the association process if the two boxes have similar feature embeddings.

An instance may have totally different appearances before and after occlusion that result in low similarity scores. As shown in Figure 8, only the front of the car appears before occlusion, while only the rear of the car appears after occlusion. Our method can associate two boxes if they cover the same discriminative regions of an object, not necessarily the exact same region. However, if two boxes cover totally

different regions of the object, they will have a low matching score.

Another corner case is the extreme high-level truncation. As shown in Figure 9, the highly truncated objects only appear a little when they just enter or leave the camera view. We cannot distinguish different instances effectively according to the limited appearance information.

E. Visualizations

We show the visualizations of different instance patches during the testing procedure in Figure 10. The detected objects in each frame are matched to prior objects via bi-directional softmax. The prior objects include tracks in the consecutive frame, vanished tracks, and backdrops. We annotate them with different colors. Each detected object is enclosed by the same color of its matched object. We can observe that most false positives in the current frame are matched to backdrops, which demonstrates keeping backdrops during the matching procedure helps reduce the number of false positives.

F. Qualitative results

We show some qualitative results of our method on BDD100K dataset and MOT17 dataset in Figure 11 and



Figure 5: Failure cases caused by inaccurate classification confidences. The objects enclosed by yellow rectangles are false negatives, and the objects enclosed by red rectangles are false positives.



Figure 6: Failure case caused by inaccurate object category. The category of the highlighted object changes from “rider” to “pedestrian” due to the occlusion of the bicycle. They cannot be associated because they do not satisfy the category consistency.



Figure 7: Inaccurate object localization caused by truncation. The red false positive box only covers part of the object, while the yellow box covers the entire object. They may have similar feature embeddings thus influencing the association procedure.

Figure 12 respectively. The results are sampled from a certain interval for illustrative purposes.

References

- [1] A. Andriyenko and K. Schindler. Multi-target tracking by continuous energy minimization. In *CVPR 2011*, pages 1265–1272. IEEE, 2011. 1
- [2] P. Bachman, R. D. Hjelm, and W. Buchwalter. Learning representations by maximizing mutual information across views. In *Advances in Neural Information Processing Systems*, pages 15535–15545, 2019. 2
- [3] P. Bergmann, T. Meinhardt, and L. Leal-Taixé. Tracking without bells and whistles. *arXiv preprint arXiv:1903.05625*, 2019. 1, 2, 5, 6, 7, 8, 9

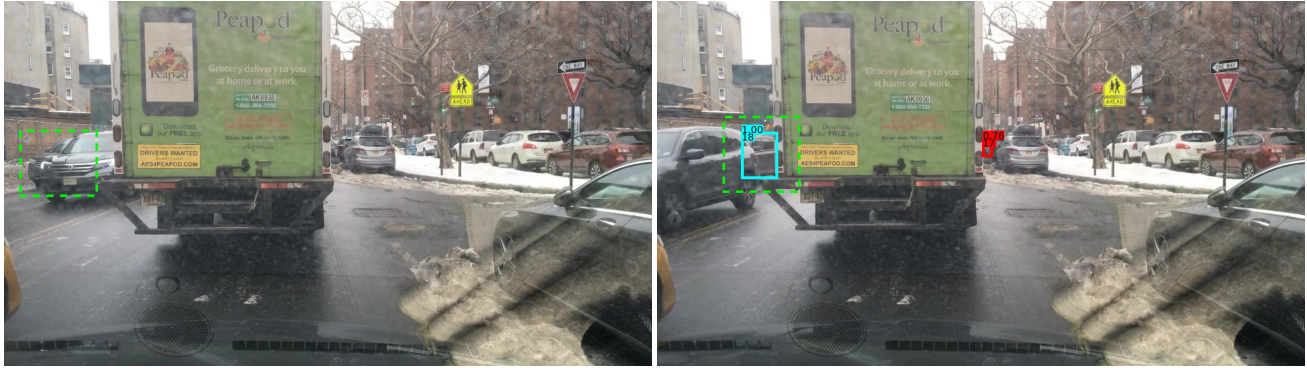


Figure 8: Two detected objects in different frames cover totally different regions of the object thus having low appearance similarity.



Figure 9: Our method cannot distinguish different instances effectively according to the limited appearance information in highly truncated objects.

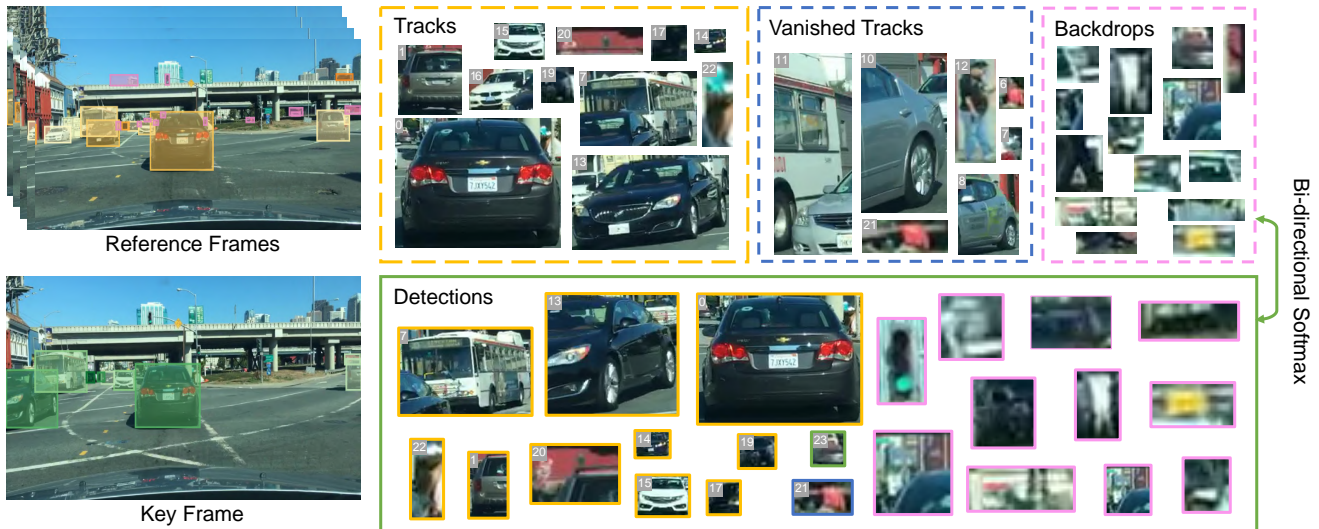


Figure 10: The visualizations of different instance patches during the testing procedure. The detected objects in the current frame are matched to tracklets in the consecutive frame, vanished tracklets, and backdrops via bi-directional softmax

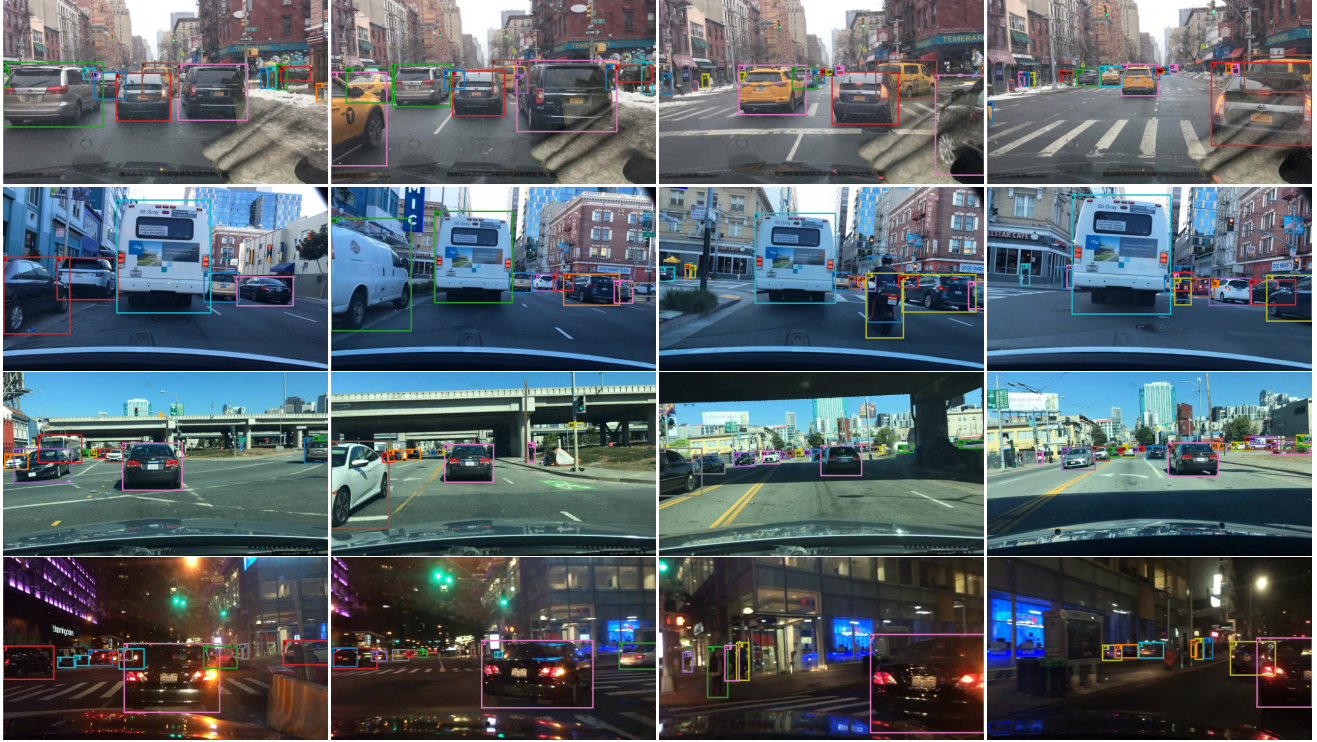


Figure 11: Qualitative results of our method on BDD100K dataset.

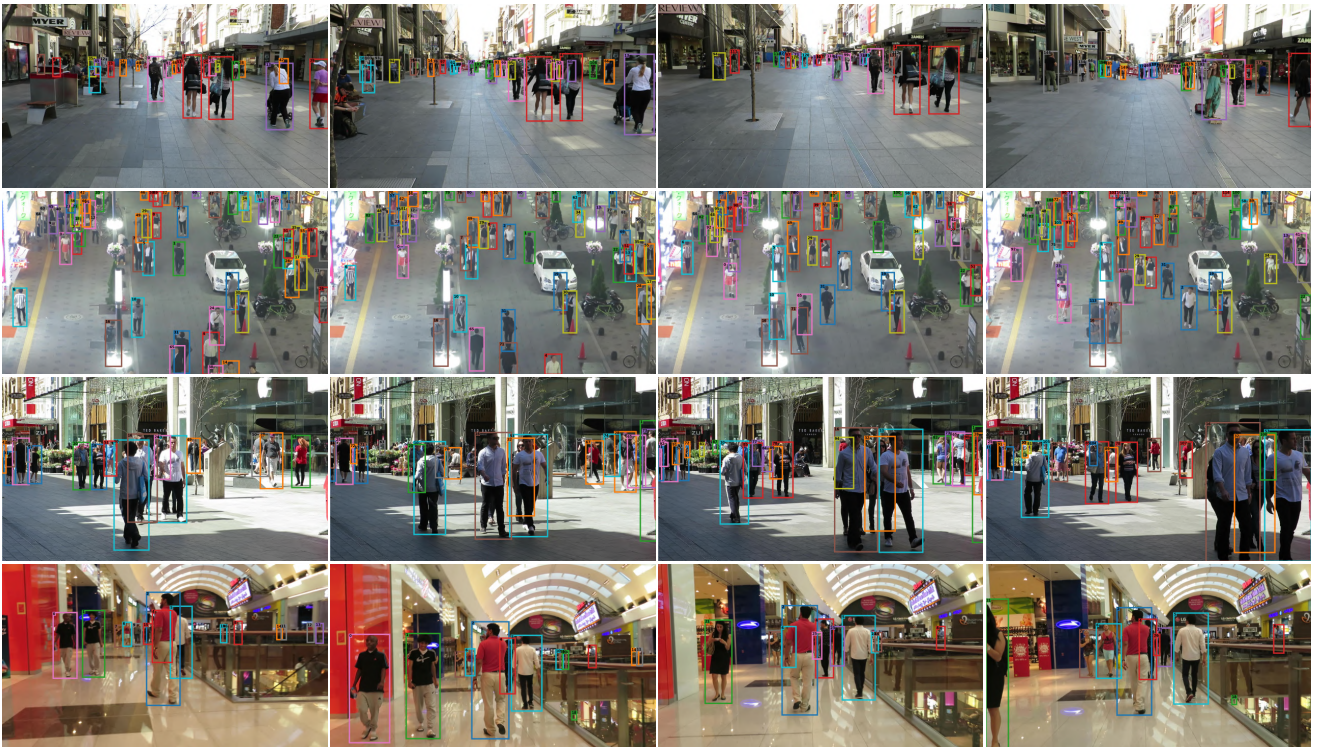


Figure 12: Qualitative results of our method on MOT17 dataset.

- [4] L. Bertinetto, J. Valmadre, J. F. Henriques, A. Vedaldi, and P. H. Torr. Fully-convolutional siamese networks for object tracking. In *European conference on computer vision*, pages 850–865. Springer, 2016. 4
- [5] A. Bewley, Z. Ge, L. Ott, F. T. Ramos, and B. Upcroft. Simple online and realtime tracking. In *International Conference on Image Processing*, 2016. 1, 2
- [6] E. Bochinski, V. Eiselein, and T. Sikora. High-speed tracking-by-detection without using image information. In *2017 14th IEEE International Conference on Advanced Video and Signal Based Surveillance (AVSS)*, pages 1–6. IEEE, 2017. 1, 2
- [7] G. Brasó and L. Leal-Taixé. Learning a neural solver for multiple object tracking. In *IEEE Conference on Computer Vision and Pattern Recognition*, 2020. 9
- [8] T. Chen, S. Kornblith, M. Norouzi, and G. Hinton. A simple framework for contrastive learning of visual representations. *arXiv preprint arXiv:2002.05709*, 2020. 2
- [9] W. Choi and S. Savarese. Multiple target tracking in world coordinate with single, minimally calibrated camera. In *European Conference on Computer Vision*, pages 553–567. Springer, 2010. 1
- [10] A. Dave, T. Khurana, P. Tokmakov, C. Schmid, and D. Ramanan. Tao: A large-scale benchmark for tracking any object. In *European Conference on Computer Vision*, 2020. 2, 5, 6, 9
- [11] M. Everingham, L. Van Gool, C. K. I. Williams, J. Winn, and A. Zisserman. The pascal visual object classes (voc) challenge. *International Journal of Computer Vision*, 88, 2010. 5
- [12] C. Feichtenhofer, A. Pinz, and A. Zisserman. Detect to track and track to detect. In *IEEE International Conference on Computer Vision*, 2017. 1, 2
- [13] A. Gupta, P. Dollar, and R. Girshick. Lvis: A dataset for large vocabulary instance segmentation. In *Proceedings of the IEEE Conference on Computer Vision and Pattern Recognition*, pages 5356–5364, 2019. 5, 6
- [14] R. Hadsell, S. Chopra, and Y. LeCun. Dimensionality reduction by learning an invariant mapping. In *2006 IEEE Computer Society Conference on Computer Vision and Pattern Recognition (CVPR'06)*, pages 1735–1742. IEEE, 2006. 2
- [15] K. He, H. Fan, Y. Wu, S. Xie, and R. Girshick. Momentum contrast for unsupervised visual representation learning. In *Proceedings of the IEEE/CVF Conference on Computer Vision and Pattern Recognition*, pages 9729–9738, 2020. 2
- [16] K. He, G. Gkioxari, P. Dollár, and R. Girshick. Mask r-cnn. In *Proceedings of the IEEE international conference on computer vision*, pages 2961–2969, 2017. 3
- [17] K. He, X. Zhang, S. Ren, and J. Sun. Deep residual learning for image recognition. In *IEEE Conference on Computer Vision and Pattern Recognition*, 2016. 2, 6
- [18] D. Held, S. Thrun, and S. Savarese. Learning to track at 100 FPS with deep regression networks. In *European Conference on Computer Vision*, 2016. 2
- [19] O. J. Hénaff, A. Srinivas, J. De Fauw, A. Razavi, C. Dorsch, S. Eslami, and A. v. d. Oord. Data-efficient image recognition with contrastive predictive coding. *arXiv preprint arXiv:1905.09272*, 2019. 2
- [20] A. Hermans, L. Beyer, and B. Leibe. In defense of the triplet loss for person re-identification. *arXiv preprint arXiv:1703.07737*, 2017. 2, 4
- [21] A. Hornakova, R. Henschel, B. Rosenhahn, and P. Swoboda. Lifted disjoint paths with application in multiple object tracking. In *International Conference on Machine Learning*, 2020. 5, 9
- [22] C. Kim, F. Li, A. Ciptadi, and J. M. Rehg. Multiple hypothesis tracking revisited. In *IEEE International Conference on Computer Vision*, 2015. 2
- [23] C. Kim, F. Li, and J. M. Rehg. Multi-object tracking with neural gating using bilinear LSTM. In *European Conference on Computer Vision*, 2018. 6
- [24] L. Leal-Taixé, C. Canton-Ferrer, and K. Schindler. Learning by tracking: Siamese CNN for robust target association. In *IEEE Conference on Computer Vision and Pattern Recognition Workshop*, 2016. 2
- [25] L. Leal-Taixé, A. Milan, K. Schindler, D. Cremers, I. Reid, and S. Roth. Tracking the trackers: an analysis of the state of the art in multiple object tracking. *arXiv preprint arXiv:1704.02781*, 2017. 2
- [26] T.-Y. Lin, P. Dollár, R. B. Girshick, K. He, B. Hariharan, and S. J. Belongie. Feature pyramid networks for object detection. In *IEEE Conference on Computer Vision and Pattern Recognition*, 2017. 3
- [27] T.-Y. Lin, M. Maire, S. Belongie, J. Hays, P. Perona, D. Ramanan, P. Dollár, and C. L. Zitnick. Microsoft coco: Common objects in context. In *European Conference on Computer Vision*, 2014. 5
- [28] Q. Liu, Q. Chu, B. Liu, and N. Yu. Gsm: Graph similarity model for multi-object tracking. In C. Bessiere, editor, *Proceedings of the Twenty-Ninth International Joint Conference on Artificial Intelligence, IJCAI-20*, pages 530–536. International Joint Conferences on Artificial Intelligence Organization, 7 2020. 9
- [29] Z. Lu, V. Rathod, R. Votel, and J. Huang. Retinatrack: Online single stage joint detection and tracking. In *IEEE Conference on Computer Vision and Pattern Recognition*, 2020. 1, 2, 6, 7
- [30] N. Mahmoudi, S. M. Ahadi, and M. Rahmati. Multi-target tracking using cnn-based features: Cnnmtt. *Multimedia Tools and Applications*, 78:7077–7096, 2018. 5
- [31] A. Milan, L. Leal-Taixé, I. Reid, S. Roth, and K. Schindler. Mot16: A benchmark for multi-object tracking. *arXiv preprint arXiv:1603.00831*, 2016. 2, 5
- [32] A. Milan, S. H. Rezatofghi, A. R. Dick, I. D. Reid, and K. Schindler. Online multi-target tracking using recurrent neural networks. In *The AAAI Conference on Artificial Intelligence*, 2017. 2
- [33] J. Munkres. Algorithms for the assignment and transportation problems. *Society for Industrial and Applied Mathematics*, 1957. 2
- [34] A. v. d. Oord, Y. Li, and O. Vinyals. Representation learning with contrastive predictive coding. *arXiv preprint arXiv:1807.03748*, 2018. 2, 3
- [35] B. Pang, Y. Li, Y. Zhang, M. Li, and C. Lu. Tubetk: Adopting tubes to track multi-object in a one-step training model. In *IEEE Conference on Computer Vision and Pattern Recognition*, 2020. 5

- [36] J. Pang, K. Chen, J. Shi, H. Feng, W. Ouyang, and D. Lin. Libra r-cnn: Towards balanced learning for object detection. In *Proceedings of the IEEE Conference on Computer Vision and Pattern Recognition*, pages 821–830, 2019. 6
- [37] J. Peng, C. Wang, F. Wan, Y. Wu, Y. Wang, Y. Tai, C. Wang, J. Li, F. Huang, and Y. Fu. Chained-tracker: Chaining paired attentive regression results for end-to-end joint multiple-object detection and tracking. In *European Conference on Computer Vision*, 2020. 1, 2, 5, 6
- [38] D. Ramanan and D. A. Forsyth. Finding and tracking people from the bottom up. In *2003 IEEE Computer Society Conference on Computer Vision and Pattern Recognition, 2003. Proceedings.*, volume 2, pages II–II. IEEE, 2003. 1, 2
- [39] S. Ren, K. He, R. Girshick, and J. Sun. Faster r-cnn: Towards real-time object detection with region proposal networks. In *Advances in Neural Information Processing Systems*, 2015. 2, 3
- [40] A. Sadeghian, A. Alahi, and S. Savarese. Tracking the untrackable: Learning to track multiple cues with long-term dependencies. In *IEEE International Conference on Computer Vision*, 2017. 2
- [41] K. Sohn. Improved deep metric learning with multi-class n-pair loss objective. In *Advances in neural information processing systems*, pages 1857–1865, 2016. 2
- [42] J. Son, M. Baek, M. Cho, and B. Han. Multi-object tracking with quadruplet convolutional neural networks. In *IEEE Conference on Computer Vision and Pattern Recognition*, 2017. 2
- [43] P. Sun, H. Kretschmar, X. Dotiwalla, A. Chouard, V. Patnaik, P. Tsui, J. Guo, Y. Zhou, Y. Chai, B. Caine, V. Vasudevan, W. Han, J. Ngiam, H. Zhao, A. Timofeev, S. Ettinger, M. Krivokon, A. Gao, A. Joshi, Y. Zhang, J. Shlens, Z. Chen, and D. Anguelov. Scalability in perception for autonomous driving: Waymo open dataset, 2019. 2, 5, 6
- [44] Y. Sun, C. Cheng, Y. Zhang, C. Zhang, L. Zheng, Z. Wang, and Y. Wei. Circle loss: A unified perspective of pair similarity optimization. *arXiv preprint arXiv:2002.10857*, 2020. 2, 3
- [45] Y. Tian, D. Krishnan, and P. Isola. Contrastive multiview coding. *arXiv preprint arXiv:1906.05849*, 2019. 2
- [46] Z. Wang, L. Zheng, Y. Liu, and S. Wang. Towards real-time multi-object tracking. *arXiv preprint arXiv:1909.12605*, 2019. 1, 2, 6
- [47] N. Wojke, A. Bewley, and D. Paulus. Simple online and real-time tracking with a deep association metric. In *International Conference on Image Processing*, 2017. 1, 2
- [48] Y. Wu and K. He. Group normalization. In *Proceedings of the European Conference on Computer Vision (ECCV)*, pages 3–19, 2018. 6
- [49] Z. Wu, Y. Xiong, S. X. Yu, and D. Lin. Unsupervised feature learning via non-parametric instance discrimination. In *Proceedings of the IEEE Conference on Computer Vision and Pattern Recognition*, pages 3733–3742, 2018. 2, 3
- [50] B. Xiao, H. Wu, and Y. Wei. Simple baselines for human pose estimation and tracking. In *Proceedings of the European conference on computer vision (ECCV)*, pages 466–481, 2018. 2
- [51] B. Yang and R. Nevatia. An online learned CRF model for multi-target tracking. In *IEEE Conference on Computer Vision and Pattern Recognition*, 2012. 2
- [52] L. Yang, Y. Fan, and N. Xu. Video instance segmentation. In *IEEE International Conference on Computer Vision*, 2019. 2, 8
- [53] F. Yu, H. Chen, X. Wang, W. Xian, Y. Chen, F. Liu, V. Madhavan, and T. Darrell. Bdd100k: A diverse driving dataset for heterogeneous multitask learning. In *The IEEE Conference on Computer Vision and Pattern Recognition (CVPR)*, June 2020. 2, 5, 6
- [54] F. Yu, W. Li, Q. Li, Y. Liu, X. Shi, and J. Yan. POI: multiple object tracking with high performance detection and appearance feature. In *European Conference on Computer Vision Workshop*, 2016. 2, 5
- [55] Y. Zhang, C. Wang, X. Wang, W. Zeng, and W. Liu. Fairmot: On the fairness of detection and re-identification in multiple object tracking. *arXiv preprint arXiv:2004.01888*, 2020. 2
- [56] X. Zhou, V. Koltun, and P. Krähenbühl. Tracking objects as points. In *European Conference on Computer Vision*, 2020. 1, 2, 5, 6, 7, 9
- [57] Z. Zhou, J. Xing, M. Zhang, and W. Hu. Online multi-target tracking with tensor-based high-order graph matching. In *2018 24th International Conference on Pattern Recognition (ICPR)*, 2018. 5